Supporting Information for "Field assessment of the wind speed-up from the two modes of dune orientation"

Ping Lü[1,*], Clément Narteau[2,*], Fang Ma[3], Jeanne Alkalla[2], Zhibao Dong[1]

[1] School of Geography and Tourism, Shaanxi Normal University, 620 Chang'an West Avenue, Xi'an, Shaanxi 710119, China.

[2] Université de Paris, Institut de physique du globe de Paris, CNRS, F-75005 Paris, France.

[3] History, Culture and Tourism School, Fuyang Normal University, Fuyang, China

[*]Corresponding authors: narteau@ipgp.fr and lvping@lzb.ac.cn

Contents

List of Figures

1 Supporting Text 1
Estimation of sand fluxes and dune properties from wind data

Transport law and shear velocity threshold

The saturated sand flux $Q_{\rm sat}$ expressed in $\mathrm{m^2\,s^{-1}}$ is computed from the shear velocity u_* using the relationship proposed by Durán, Claudin, and Andreotti (2011) and Kok, Parteli, Michaels, and Karam (2012),

$$Q_{\rm sat}(u_*) = \begin{cases} A_{\rm v}\,\dfrac{\rho_{\rm f}}{\rho_{\rm s} g} u_{\rm c}\left(u_*^2 - u_{\rm c}^2\right) & \text{for } u_* > u_{\rm c}, \\ 0 & \text{else,} \end{cases} \tag{1}$$

where the prefactor $A_{\rm v} \approx 8.33$ takes into account a dune compactness of 0.6 in order to easily convert sand fluxes into effective dune properties (e.g., volume, migration rates). In this formula, $u_{\rm c}$ is the threshold shear velocity. Its value is determined from

$$u_{\rm c} = A\sqrt{\frac{\rho_{\rm s} - \rho_{\rm f}}{\rho_{\rm f}} g d}, \tag{2}$$

using $A = 0.082$ to consider only the impact threshold, the lowest shear rate at which saltation can be maintained after it has been initiated (Bagnold, 1941).

Sand flux on a flat bed from wind data

We use the surface wind data from the ECMWF ERA5-Land reanalysis (Hersbach et al., 2019). This global meteorological forecasting model based on assimilation aims to include all available and appropriate observational data from weather station, radiosonde, ship and satellite measurements. It provides numerical predictions from the beginning of 1950 up to now with a horizontal spatial resolution of $0.1^\circ \times 0.1^\circ$ (about 11 km on the equator) and a time resolution of 1 hour. Wind data provide the wind speed u and direction θ at a height $z = 10$ m and at different times t_i, $i \in [1; N]$. The shear velocity of a flat sand bed can be extrapolated using the law of the wall,

$$u_{\rm flat} = u\frac{\kappa}{\log(z/z_{\rm a})}, \tag{3}$$

where κ the is the von-Kármán constant. Instead of the geometric roughness that depends only on grain size, we consider here the aerodynamic roughness $z_{\rm a}$ that accounts for the height of the transport layer in which saltating grains modify the vertical wind velocity profile. The mean shear velocity, $\langle u_* \rangle$, is defined as the shear velocity averaged over the transport periods,

$$\langle u_* \rangle = \frac{\sum_{i=1}^{N} u_{\rm flat} H_u}{\sum_{i=1}^{N} H_u} \qquad \text{where} \qquad H_u = \begin{cases} 1 & \text{for } u_{\rm flat} > u_{\rm c}, \\ 0 & \text{else.} \end{cases} \tag{4}$$

Using Equation 1, we compute the saturated sand flux vector on a flat sand bed,

$$\overrightarrow{Q}_{\rm flat} = \begin{bmatrix} Q_{\rm sat}(u_{\rm flat})\cos(\theta) \\ Q_{\rm sat}(u_{\rm flat})\sin(\theta) \end{bmatrix}. \tag{5}$$

For the entire time period, we estimate the resultant sand flux on a flat erodible bed:

$$\langle \overrightarrow{Q}_{\text{flat}} \rangle = \frac{1}{N} \sum_{i=1}^{N} \overrightarrow{Q}_{\text{flat}}. \tag{6}$$

According to Fryberger and Dean (1979), we estimate the resultant drift potential

$$\text{RDP} = \left\| \langle \overrightarrow{Q}_{\text{flat}} \rangle \right\| = \left\| \frac{1}{N} \sum_{i=1}^{N} \overrightarrow{Q}_{\text{flat}} \right\|. \tag{7}$$

and the direction of $\langle \overrightarrow{Q} \rangle$ is usually called the resultant drift direction (RDD). The latter is also referred to as the resultant transport direction. These two quantities are highly dependent on the wind directionality because the contributions of winds from opposite directions cancel each other out. We also calculate the drift potential,

$$\text{DP} = \frac{1}{N} \sum_{i=1}^{N} \| \overrightarrow{Q}_{\text{flat}} \|, \tag{8}$$

Unlike the resultant drift potential, this mean sand flux does not take into account the orientation of the individual sand fluxes computed from the successive wind measurements. The ratio RDP/DP is a non-dimensional parameter, which is often used to characterize the directional variability of the wind regimes (Fryberger & Dean, 1979; Pearce & Walker, 2005): RDP/DP $\rightarrow 1$ indicates that sand transport tends to be unidirectional; RDP/DP $\rightarrow 0$ indicates that most of the transport components cancel each other out.

Sand flux at the crest of dunes from wind data

To compute the wind speed at the crest for all wind directions θ and all dune orientations α, we consider an infinite and symmetric linear dune with of triangular shape with base $2L$ and height H. Then, $H\left|\sin\left(\theta-\alpha\right)\right|/L$ is the apparent dune aspect-ratio as seen by the wind, and according to Equations. 1 and 2 of the main manuscript

$$u_{\text{crest}}(\alpha) = u_{\text{flat}}\left(1+\delta\left|\sin\left(\theta-\alpha\right)\right|\right), \qquad \text{where} \qquad \delta = \beta\frac{H}{L}. \tag{9}$$

Note that in the main manuscript, according to our triangular dune shape, $\mathcal{L} = L/2$. In Equation 9, the estimation of u_{crest} does not take into account the change in dune shape after each wind reversal (i.e., no crest reversal) nor a difference in slope between both sides of the dune. We assume that there is no wind deflection on the dune (Figure S4), so that the flow at the crest is a horizontal vector that can be decomposed into a parallel-to-crest and a normal-to-crest components of transport*

$$\overrightarrow{Q}_{\text{crest}}(\alpha) = \begin{bmatrix} Q_{\parallel}(\alpha) \\ Q_{\perp}(\alpha) \end{bmatrix} = \begin{bmatrix} Q_{\text{sat}}\big(u_{\text{crest}}(\alpha)\big)\cos\left(\theta-\alpha\right) \\ Q_{\text{sat}}\big(u_{\text{crest}}(\alpha)\big)\sin\left(\theta-\alpha\right) \end{bmatrix}. \tag{10}$$

For the entire time period and for all dune orientations α, we can compute the parallel-to-crest and normal-to-crest components of the resultant sand flux at the crest

$$\langle \overrightarrow{Q}_{\text{crest}}(\alpha) \rangle = \frac{1}{N} \begin{bmatrix} \sum_{i=1}^{N} Q_{\parallel}(\alpha) \\ \sum_{i=1}^{N} Q_{\perp}(\alpha) \end{bmatrix} = \frac{1}{N} \begin{bmatrix} \sum_{i=1}^{N} Q_{\text{sat}}\big(u_{\text{crest}}(\alpha)\big)\cos\left(\theta-\alpha\right) \\ \sum_{i=1}^{N} Q_{\text{sat}}\big(u_{\text{crest}}(\alpha)\big)\sin\left(\theta-\alpha\right) \end{bmatrix}. \tag{11}$$

*The components of sand flux vectors in the parallel-to-crest and normal-to-crest unit vectors are shown in [ ].

Since dunes build up from sand fluxes perpendicular to the crest, the dune growth rate is expressed in units of sand flux as the sum of all the normal-to-crest components of transport, i.e.,

$$\sigma(\alpha) = \frac{1}{N}\sum_{i=1}^{N} |Q_{\perp}(\alpha)| = \frac{1}{N}\sum_{i=1}^{N} Q_{\mathrm{sat}}(u_{\mathrm{crest}}(\alpha))\,|\sin(\theta-\alpha)\,|. \tag{12}$$

Dunes in the bed instability mode

In zones with no limit in sand availability, dune growth is governed by the flat bed instability (Gadal, Narteau, du Pont, Rozier, & Claudin, 2019; Lü et al., 2021). Under such transport-limited conditions, periodic dune patterns increase in amplitude perpendicularly to the direction for which the normal-to-crest component of transport is maximum (Rubin & Hunter, 1987). In practice, the orientation $\alpha_{\mathrm{H}} \in [0;\pi]$ for which the growth rate reaches its maximum σ_{H} determines the alignment of dunes in the bed instability mode, i.e.,

$$\frac{\mathrm{d}\sigma(\alpha)}{\mathrm{d}\alpha} = \frac{\mathrm{d}\sum_{i=1}^{N} |Q_{\perp}(\alpha)|}{\mathrm{d}\alpha} = 0. \tag{13}$$

This procedure is also known as the gross bedform-normal transport rule, except that we take into account the speed-up effect. The resultant sand flux at the crest of dunes in the bed instability mode is

$$\langle \overrightarrow{Q}_{\mathrm{H}} \rangle = \langle \overrightarrow{Q}_{\mathrm{crest}}(\alpha_{\mathrm{H}}) \rangle. \tag{14}$$

Its orientation α_{M} and magnitude $\|\langle \overrightarrow{Q}_{\mathrm{H}} \rangle\|$ can be used to compute the overall transport perpendicular to the crest (see also Equation 11),

$$\|\langle \overrightarrow{Q_{\mathrm{M}}} \rangle\| = \|\langle \overrightarrow{Q_{\mathrm{H}}} \rangle\| \times |\sin(\alpha_{\mathrm{M}} - \alpha_{\mathrm{H}})|, \tag{15}$$

in order to estimate the migration rate of dunes in the bed instability mode.

Dunes in the elongating mode

In zones with low sand availability under multidirectional wind regimes, dunes can elongate in the direction of the resultant sand flux at the crest (Zhang, Narteau, Rozier, & Courrech du Pont, 2012; Courrech du Pont, Narteau, & Gao, 2014; Gao, Narteau, Rozier, & Courrech du Pont, 2015). The direction of elongation $\alpha_{\mathrm{E}} \in [0;2\pi]$ is the one for which the normal-to-crest components of transport cancel each other out and for which the sum of the parallel-to-crest components is positive, i.e.,

$$\sum_{i=1}^{N} Q_{\perp}(\alpha) = 0 \qquad \text{and} \qquad \sum_{i=1}^{N} Q_{\parallel}(\alpha) > 0. \tag{16}$$

The resultant sand flux at the crest of elongating dunes is

$$\langle \overrightarrow{Q}_{\mathrm{E}} \rangle = \langle \overrightarrow{Q}_{\mathrm{crest}}(\alpha_{\mathrm{E}}) \rangle \tag{17}$$

By definition, its magnitude $\|\langle \overrightarrow{Q}_{\mathrm{E}} \rangle\| = \|\langle \overrightarrow{Q}_{\mathrm{crest}}(\alpha_{\mathrm{E}}) \rangle\|$ is the parallel-to-crest component of transport (see also Equation 11), which can be used to compute the elongation rate (Lucas et al., 2015). Considering the speed-up effect ($\delta \neq 0$), the direction of elongation (i.e., α_{E}) may differ from the resultant transport direction on a flat sand bed (Rozier, Narteau, Gadal, Claudin, & Courrech du Pont, 2019). According to Equation 12, $\sigma_{\mathrm{E}} = \sigma(\alpha_{\mathrm{E}})$.

Figure S1: Dune patterns on the alluvial fan of the Nalinggele River. **(a)** Overview of the instrumented elongating dune from the hillside from which it elongates. **(b)** Periodic dune pattern of small amplitude in a coarse-grain area south of the instrumented elongating dune. **(c)** Overview of the elongating dune field west of the active bed of the Nalinggele River. **(d)** Coarse grain area between two elongating dunes. **(e)** Barchanoid ridges northwest of the elongating dune field. **(f)** Active dune collapsing along a terrace of the Nalinggele River. See Figure 1a in the main manuscript to have an overview of all these sites. All pictures were taken on October 25, 2023.

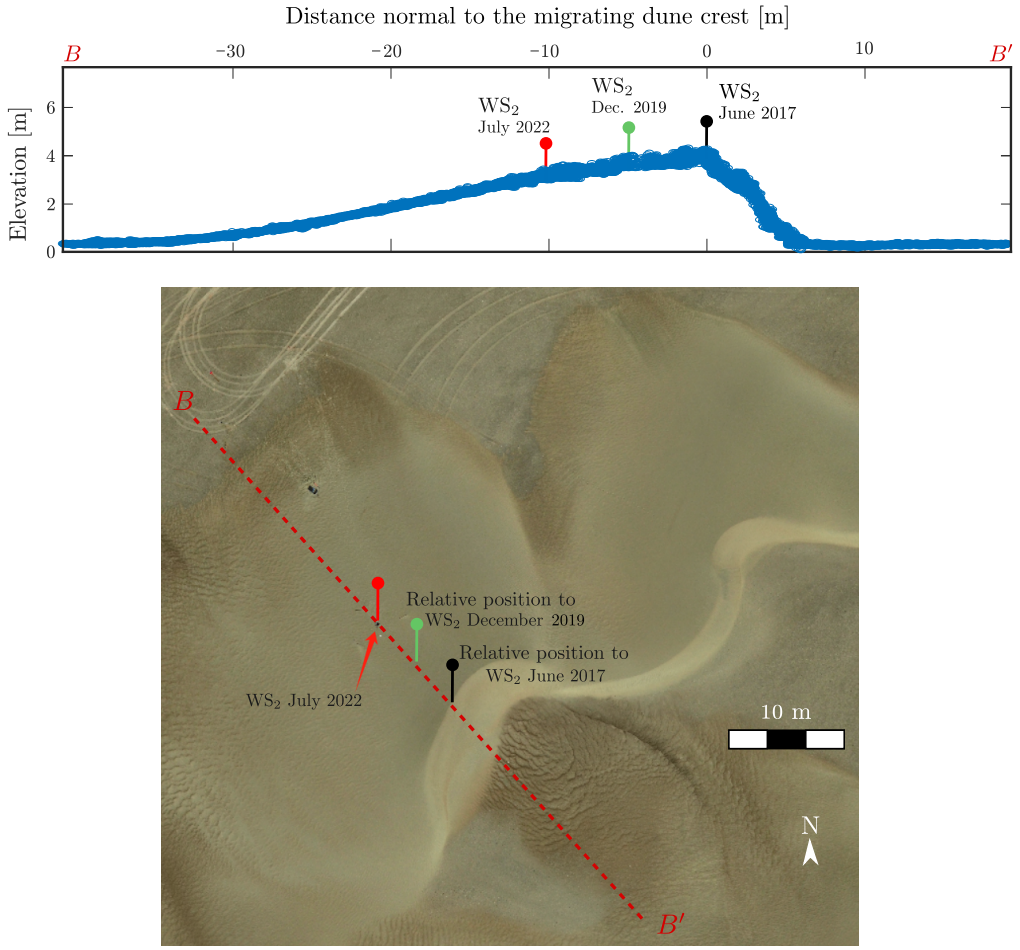

Figure S2: Evolution of the position of the anemometer on the migrating dune. Relative position of the anemometer to the crest of the migrating dune at three different times (top). This position is reported on a picture taken on 7 July 2022 from a drone (bottom). In both cases, a steady-state dune migration is assumed.

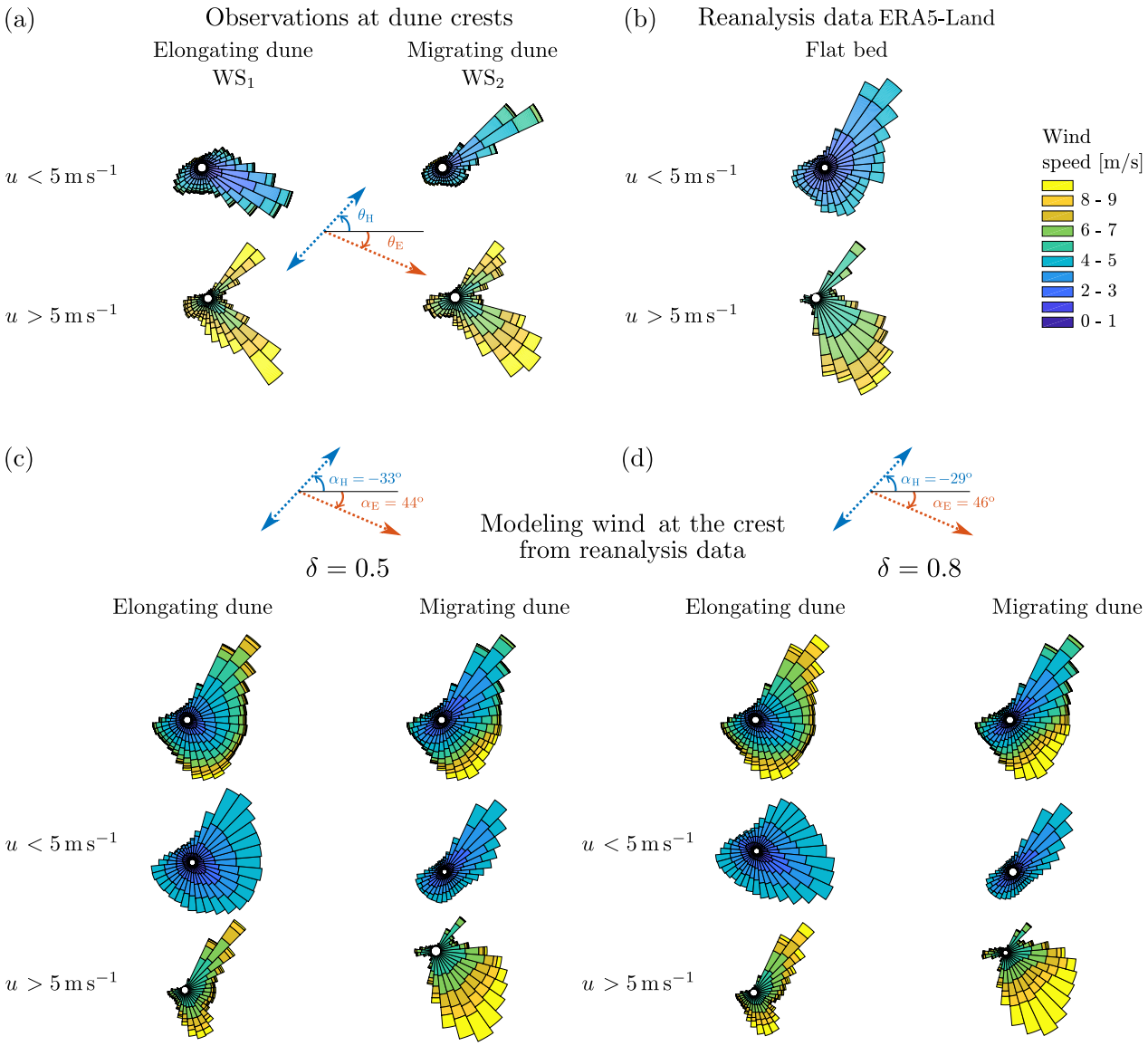

Figure S3: Comparison between the wind roses measured at the crest of elongating and migrating dunes and those predicted from the dune model using the ERA5-Land data (a) Field-measured wind roses at the crest of the elongating (left) and migrating (right) dunes for wind speed less (top) and greater (bottom) than 5 $\mathrm{m\,s^{-1}}$. θ_H and θ_E are the observed dune crest alignment of the migrating and elongating dunes, respectively. **(b)** ERA5-Land wind roses for wind speed less (top) and greater (bottom) than 5 $\mathrm{m\,s^{-1}}$. **(c,d)** ERA5-Land wind roses at the crest of elongating (left) and migrating (right) dunes using the model described in Supporting Text 1 and δ-values of 0.5 (c) and 0.8 (d). α_H and α_E are the predicted dune crest alignment of the migrating and elongating dunes, respectively. For a direct comparison with field-measured wind roses shown in (a), wind speed less (top) and greater (bottom) than 5 $\mathrm{m\,s^{-1}}$ are distinguished.

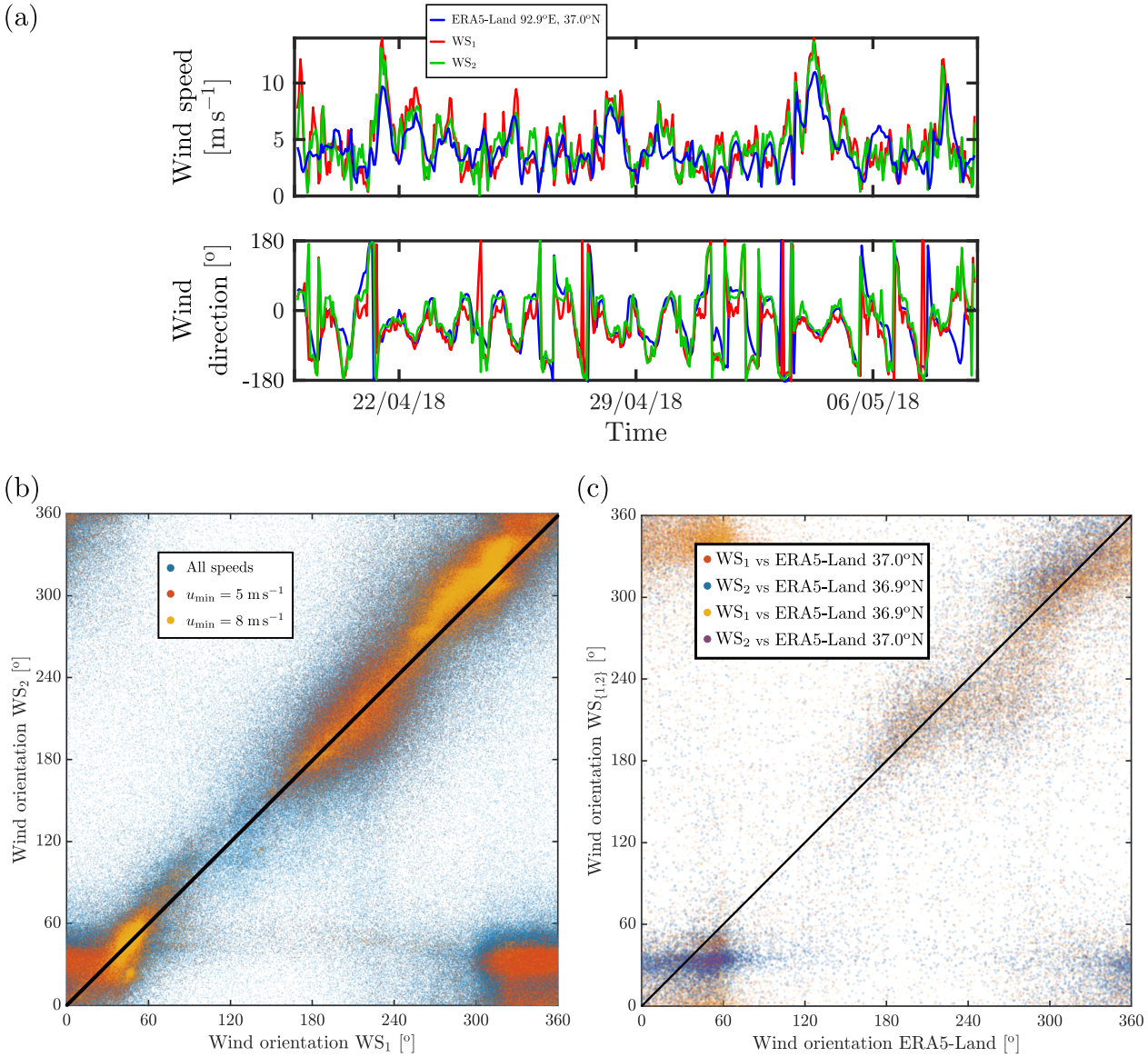

Figure S4: Comparison of wind orientation at the crest of dunes. **(a)** Wind speed (top) and orientation (bottom) from the ERA-Land climate reanalysis and field measurements at the crest of the elongating (left) and migrating (right) dunes. **(b)** Comparison of wind orientation at the crest of the elongating (left) and migrating (right) dunes for different ranges of wind speed. **(c)** Comparison between the orientation of the surface wind of the ERA-Land climate reanalysis at two location, (92.9°E, 36.9°N) and (92.9°E, 37°N), and wind orientation at the crest of the elongating (left) and migrating (right) dunes.

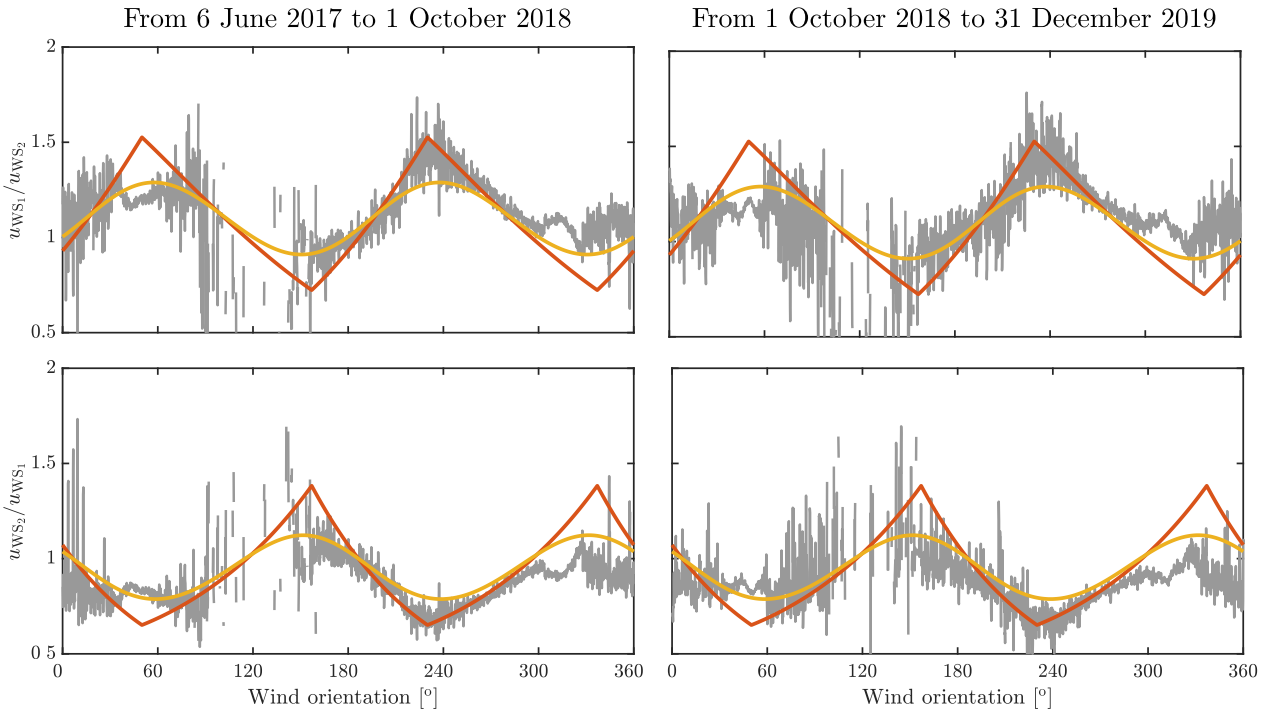

Figure S5: Wind speed ratio at the crest of dunes as a function of wind direction for different time periods. Gray dots show the median of the distribution of the wind-speed ratio with respect to wind direction for two time periods of similar duration ($\approx$ 460 days). These distributions are computed every 0.1° using a sliding window algorithm with an angular range of 0.2°. Only times with wind speeds greater than 8 $\mathrm{m\,s^{-1}}$ for at least one wind measurement are used. These data are compared with the model presented in Equation 4 using the best estimates of the $\{\beta_1, \beta_2\}$-values for the entire time period (Figure S7). There is no significant change between the distributions obtained over the initial (left) and final (right) time periods, indicating that the data is not precise enough to capture the change in the position of the anemometer relative to the dune crest on the migrating dune. No migration is expected for the elongating dune, as it is attached to a topographic obstacle upstream (Courrech du Pont et al., 2014; Lucas et al., 2015; Rozier et al., 2019).

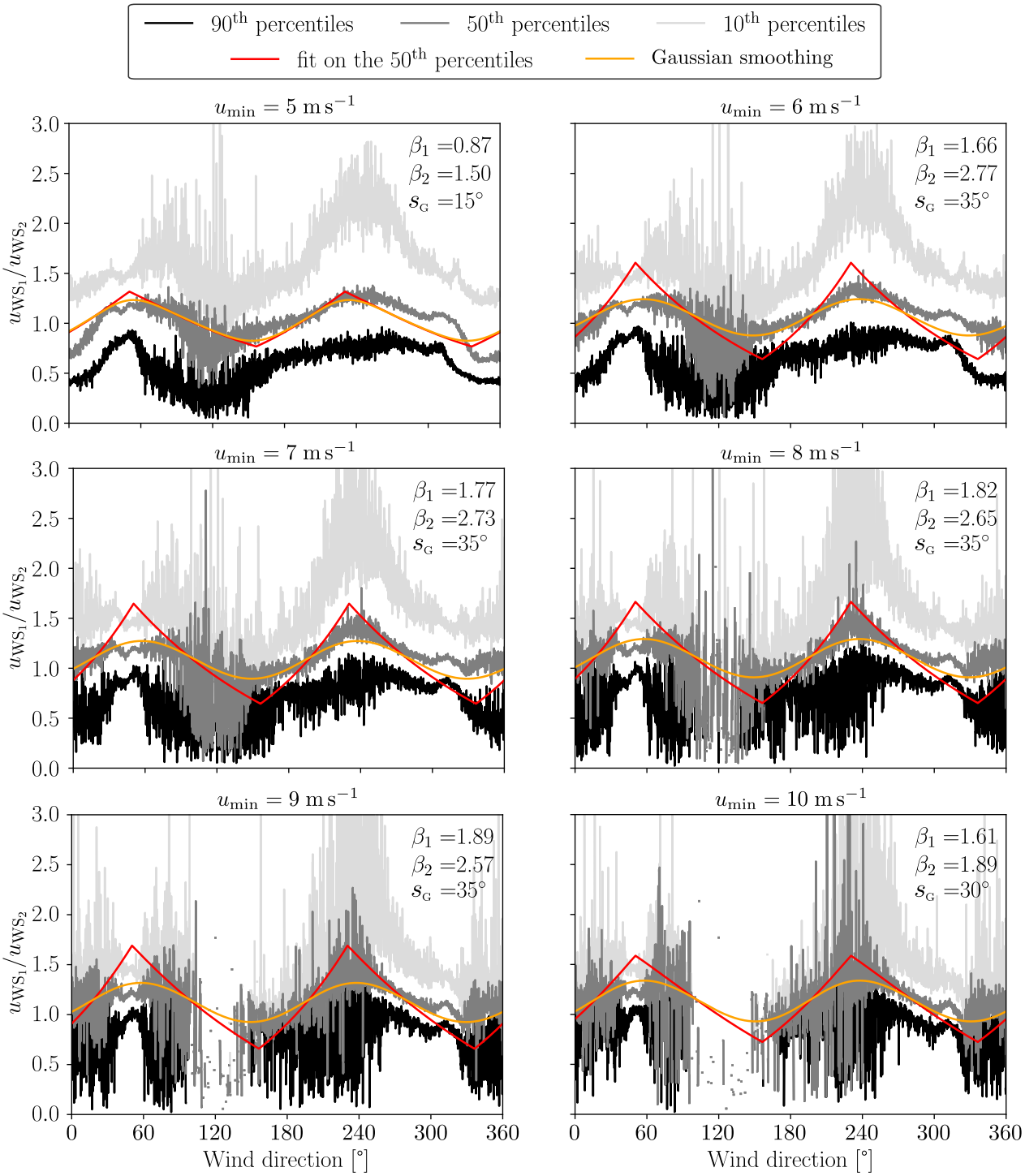

Figure S6: Wind speed ratio at the crest of dunes as a function of wind direction for different ranges of wind speed. Gray dots show quantiles of the distribution of the wind-speed ratio with respect to wind direction. These distributions are computed every 0.1° using a sliding window algorithm with an angular range of 0.2°. Only times with wind speeds greater than u_{min} for at least one wind measurement are used. These data are compared with the model presented in Equation 4 using the best estimates of the $\{\beta_1, \beta_2\}$-values (Figure S7). The agreement between the model and the data is better for wind directions between 240° and 300° when the northerly wind hits the northern side of the elongating dunes. The smoothed version of the model is better for wind directions ranging in $[-60°, 90°]$ when northwesterly winds and westerly winds hits the southern side of the elongating dunes and the stoss slope of the migrating barchan. This is because the model considers a triangular dune and does not take into account the rounded shape of the barchan or the raked pattern that develops on the southern side of the elongating dune.

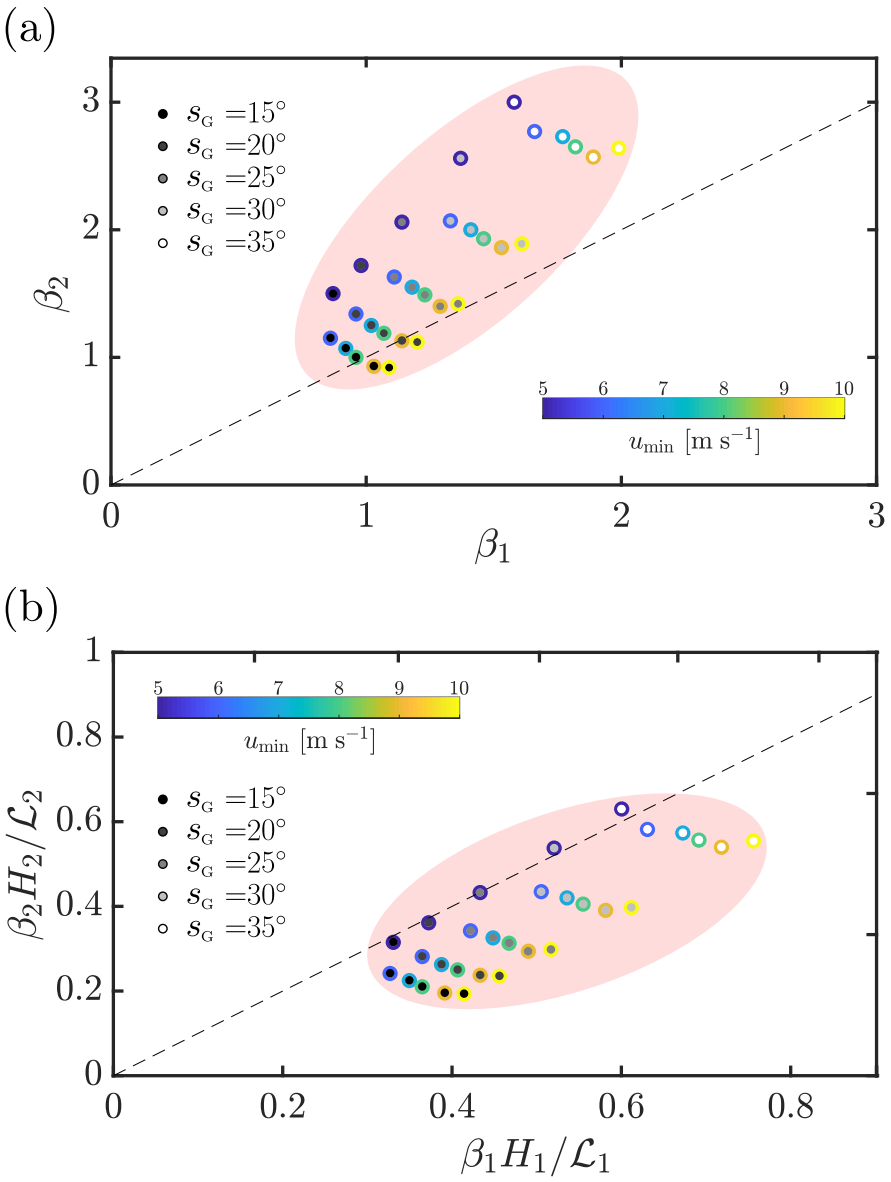

Figure S7: Estimation to the fractional speed-up ratio. **(a)** Best estimates of the $\{\beta_1, \beta_2\}$-values using Equation 4 of the main manuscript, for different minimum wind speed, u_m, and different Gaussian smoothing, s_G. **(b)** Values of the fractional speed-up ratio, δ, for the elongating and migrating dunes using the $\{\beta_1, \beta_2\}$-values and the dune aspect-ratio measured on the dunes (Figure 2a of the main manuscript). Based on these estimates, dune orientations and the associated sand fluxes are computed for $\delta \in [0.3, 0.6]$ (Table 1 and Figure 4 of the main manuscript).

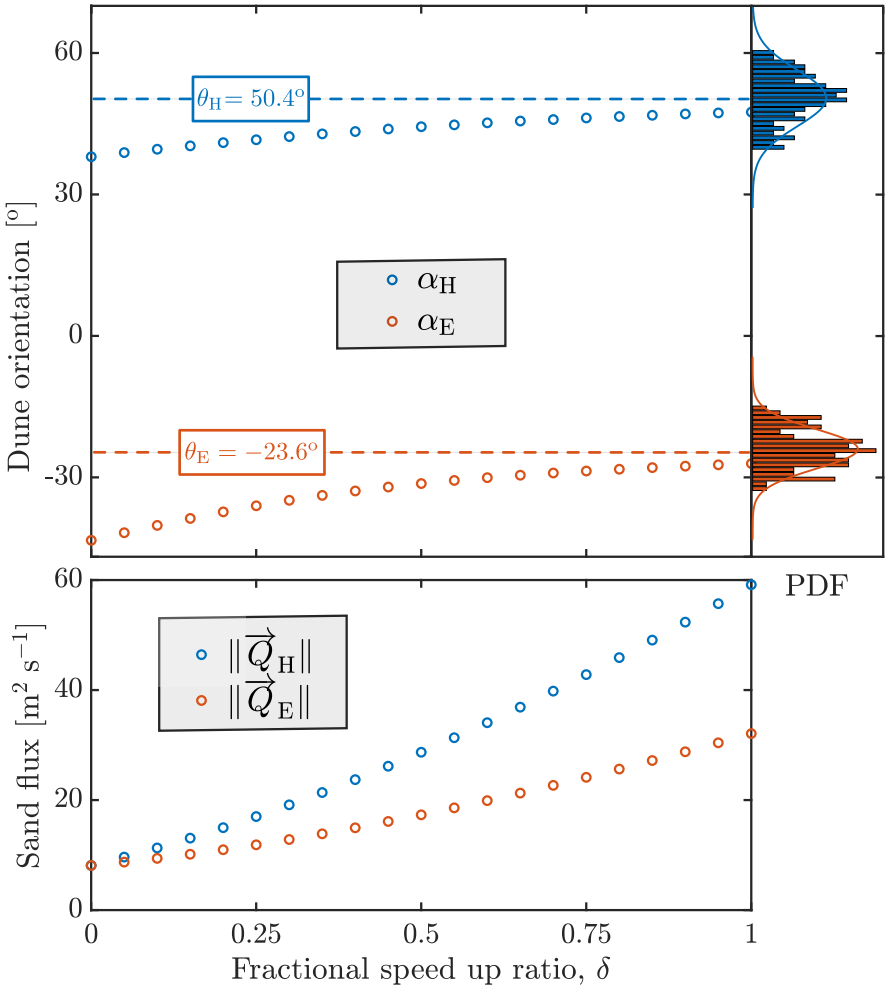

Figure S8: Dune orientations and sand fluxes with respect to the fractional speed-up ratio. All variables are computed using the formalism described in Supporting Text 1. Dune orientations, $\{\alpha_H, \alpha_E\}$, are compared to the observed dune orientations $\{\theta_H, \theta_E\}$. Sand fluxes, $\{\|\vec{Q}_H\|, \|\vec{Q}_E\|\}$, are used to compute the migrating rate of barchanoid ridges and the elongating rate of linear dunes shown in Figure 4 of the main manuscript.

References

Bagnold, R. A. (1941). *The Physics of Blown Sand and Desert Dunes.* London: Chapman and Hall.

Courrech du Pont, S., Narteau, C., & Gao, X. (2014). Two modes for dune orientation. *Geology*, *42*(9), 743–746.

Durán, O., Claudin, P., & Andreotti, B. (2011). On aeolian transport: grain-scale interactions, dynamical mechanisms and scaling laws. *Aeolian Research*, *3*(3), 243–270.

Fryberger, S. G., & Dean, G. (1979). Dune Forms and Wind Regime. *A Study of Global Sand Seas*, *1052*, 137–169.

Gadal, C., Narteau, C., du Pont, S. C., Rozier, O., & Claudin, P. (2019). Incipient bedforms in a bidirectional wind regime. *Journal of Fluid Mechanics*, *862*, 490–516.

Gao, X., Narteau, C., Rozier, O., & Courrech du Pont, S. (2015). Phase diagrams of dune shape and orientation depending on sand availability. *Scientific Reports*, *5*, 14677.

Hersbach, H., Bell, W., Berrisford, P., Horányi, A., Muñoz-Sabater, J., Nicolas, J., ... Dee, D. (2019, 04). Global reanalysis: goodbye ERA-Interim, hello ERA5. *ECMWF Newsl*, 17-24.

Kok, J. F., Parteli, E. J., Michaels, T. I., & Karam, D. B. (2012). The physics of wind-blown sand and dust. *Reports on progress in Physics*, *75*(10), 106901.

Lü, P., Narteau, C., Dong, Z., Claudin, P., Rodriguez, S., An, Z., ... Courrech du Pont, S. (2021). Direct validation of dune instability theory. *Proceedings of the National Academy of Sciences*, *118*(17). doi: 10.1073/pnas.2024105118

Lucas, A., Narteau, C., Rodriguez, S., Rozier, O., Callot, Y., Garcia, A., & Courrech du Pont, S. (2015). Sediment flux from the morphodynamics of elongating linear dunes. *Geology*, *43*, 1027–1030.

Pearce, K. I., & Walker, I. J. (2005). Frequency and magnitude biases in the 'Fryberger' model, with implications for characterizing geomorphically effective winds. *Geomorphology*, *68*(1), 39–55.

Rozier, O., Narteau, C., Gadal, C., Claudin, P., & Courrech du Pont, S. (2019). Elongation and stability of a linear dune. *Geophysical Research Letters*, *46*, 14521–14530.

Rubin, D., & Hunter, R. E. (1987). Bedform alignment in directionally varying flows. *Science*, *237*(4812), 276–278.

Zhang, D., Narteau, C., Rozier, O., & Courrech du Pont, S. (2012). Morphology and dynamics of star dunes from numerical modelling. *Nature Geoscience*, *5*(7), 463–467.